Solar-Terrestrial Physics. 2024. Vol. 10. Iss. 3. P. 18–24. DOI: 10.12737/stp-103202403. © 2024 N.E. Ovchinnikova, V.M. Bogod, M.K. Lebedev. Published by INFRA-M Academic Publishing House

UDC 523.98
DOI: 10.12737/stp-103202403

Received March 30, 2024
Accepted May 23, 2024

OBSERVATION AT RADIO FREQUENCIES OF THE HYDROXYL (OH) ABSORPTION LINE IN FILAMENTS AND PROMINENCES ABOVE ACTIVE REGIONS OF THE SUN

N.E. Ovchinnikova
Special Astrophysical Observatory, St. Petersburg, Russia, n.e.ovchinnikova@gmail.com

M.K. Lebedev
Special Astrophysical Observatory, St. Petersburg, Russia, m.k.lebedev@gmail.com

V.M. Bogod
Special Astrophysical Observatory, St. Petersburg, Russia, vbog_spb@mail.ru

Abstract. When observing the Sun with RATAN-600 radio telescope using a spectropolarimetric complex in the range 1–3 GHz, as well as when observing coronal rain, absorption in the radio emission was discovered in the spectral region 1.5–1.65 GHz in active solar regions located under a cold filament or on the limb under a prominence. The observed line structure corresponds to the hyperfine splitting frequencies in the ground state of $X^2\Pi_{3/2}$ hydroxyl (OH) 1612–1720 MHz. When the observed active region passes through the knife-shaped beam pattern of the telescope antenna, the absorption band shifts in frequency due to a shift in the energy levels of the OH molecule in a magnetic field, which changes along the filament.

Keywords: Sun, coronal structures, absorption lines, hydroxyl.

INTRODUCTION

Studying the spectrum of physical objects allows us to understand their intrinsic nature. Spectroscopic observations of the Sun are made in the photosphere and chromosphere since observations of the corona in optical ranges are limited by low plasma density, high temperature (~10^6 K), and insufficient sensitivity of existing instruments.

The search for atomic hydrogen emission lines has been conducted for a long time [Wild, 1952; Khersonskii, Varshalovich, 1980; Dravskih, Dravskih, 2022]. Hydroxyl (OH) absorption lines on the Sun are observed in the photosphere in the IR range; detection of hydroxyl is considered a marker of the presence of molecular hydrogen [Jaeggli et al., 2012]. This allows us to assume the presence of hydroxyl in cold structures in the corona (filaments, prominences, and coronal rain) and to expect the possibility of detecting its lines in the radio frequency range. Radio emission of active regions (AR) on the Sun is determined by the structure of strong magnetic fields of the solar corona, in which the Zeeman effect leads to measurable atomic level splitting and polarization of the emitted light [Derouich, 2017]. However, modern instruments operating in the radio frequency range do not have either sufficient frequency resolution or sufficient sensitivity to observe the fine radiation structure of individual coronal formations.

1. SPECTRAL OBSERVATIONS WITH RATAN-600 IN THE 1–3 GHz RANGE

The data obtained with the spectropolarimetric solar complexes of the RATAN-600 telescope represents a time series of spectrograms of solar radio emission in the 1–18 GHz range. Parameters of the 1–3 GHz complex [Ripak et al., 2023]:

- maximum frequency resolution — 122 kHz;
- total number of frequency channels — 2×8192;
- measured polarizations — right- and left-hand circular;
- time resolution — 8 ms/spectrum;
- input noise temperature — 100–300 K;
- dynamic range — 30–60 dB (30 dB — DSP system, 60 dB — stepped attenuators);
- frequency averaging — 8–64 times (128–1024 channel/GHz);
- output frequency resolution — 1–8 MHz;
- capability of studying the dynamics of the process in the mode of multiple 10-min tracking of a selected object on the solar disk.

Due to the large dynamic range and high time resolution of the receiving system of the complex (approximately 119 spectra per second in the entire frequency range) when scanning the Sun with the antenna beam along the parallel of declination, variations in the spectral radio emission flux density are recorded at the level of 0.1 solar flux unit (10^3 Jy) within the beam width. These variations are caused by active coronal structures within the area covered by the beam pattern at each frequency. In the 1–3 GHz frequency range, the width of the beam pattern (BP) of the RATAN-600 antenna system (AS) “South sector + Periscope” strongly depends on the wavelength (from 84″ to 252″), and the AS spatial resolution varies threefold. Therefore, when working in a wide frequency range, observational data is subjected to deconvolution with a theoretical hori-

This is an open access article under the CC BY-NC-ND license

zontal BP, calculated by the aperture integration method. As a result, the radio image of the sources whose width is more than a quarter of the beam width is reduced to its true width at corresponding wavelengths, which allows point sources located in close proximity to them to be resolved provided that the ratio of the flux from the point source to the background exceeds the ratio of noise power to background signal power (in our measurements it is 10^{-3}). Dimensions of the reconstructed radio image of the point source do not exceed a quarter of the beam width; the integral spectral flux density from the source remains unchanged.

When conducting observations at high resolution (1 MHz) and in the mode of tracking of the selected AR, the feed of the complex is set exactly in the focus of AS, whereas during multi-azimuth observations in the standard mode at a 4 MHz resolution, the feed is offset from the focus by 430 mm. Spectrograms of the horizontal BP of the RATAN-600 AS "South sector + Periscope" for both positions of the 1–3 GHz feed are presented in Figure 1, *a*, *b* respectively.

In the tracking mode, recording is carried out similarly to the transit mode within the width of the horizontal antenna BP. Tracking is used to increase sensitivity through time signal accumulation.

To process multifrequency data, we employ factor analysis methods [Smilde et al., 2005], in particular the principal component analysis (PCA) based on singular value decomposition (SVD), which has long been used in spectroscopy (specifically in astrophysics) [Heyer, Schloerb, 1997].

As to solar radio emission data, when the PCA is applied, the following components sequentially emerge: a slowly varying component (emission from the quiet Sun and AR thermal bremsstrahlung, manifested at all frequencies); spectral components that vary rapidly in time or are localized in frequency, such as bursts, emission or absorption lines; local interference and satellite signals, and, finally, Gaussian noise components.

The spectral flux density data is calibrated using the flux spectrum of the quiet Sun, i.e. the spectrum of the solar radio emission flux during solar minimum. To calculate the part of the spectral flux density of the quiet Sun received by the RATAN-600 AS "South sector + Periscope", we use data from the Nobeyama Radio Polarimeter (NoRP) and the Radio Solar Telescope Network (RSTN), as well as data on the microwave radio brightness temperature spectrum of the quiet Sun [Zirin et al., 1991]. The observations are calibrated under the assumption that the values thus calculated are the spectra of the first principal component in the PCA decomposition.

2. OBSERVATIONAL RESULTS AND DISCUSSION

For the first time, the component with an absorption line in its spectrum was detected in our observations in December 2021 when we processed test measurements of the new complex with a resolution of 1 MHz.

The absorption line was observed in March and June 2022 [Ovchinnikova et al., 2022], March, May, and September 2023, January–March 2024. The observations were carried out both in transit and tracking modes with a resolution from 1 to 4 MHz.

The energy level splitting in the magnetic field is due to breaking of the degeneracy between the levels with different magnetic quantum numbers. The interaction of the magnetic moment with the field changes the energy level depending on the mutual orientation of the magnetic moment and the field. In the OH molecule, for each of the Λ-doubling splitting of a ground state $X^2\Pi_{3/2}$, the lower sublevel is split into three; the upper one, into five Zeeman sublevels. According to the selection rules, transitions with a change in the magnetic quantum number ΔM_J=0, ±1 are allowed. The structure of the OH molecule energy levels is such that when the external magnetic field is superposed for transitions with ΔM_J=+1 the component σ^- arises with a frequency lower than the initial transition frequency. Using the scheme of energy levels [Maeda et al., 2015], for values of *B* within several tens of Gauss we can estimate this change at 1.4–1.5 MHz/G. To transitions with ΔM_J=–1 corresponds the σ^+ component shifted toward a higher frequency. If the field exceeds 20–25 G, the frequency shift is 35–40 MHz and its emission falls into the band of the receiver's choke filter.

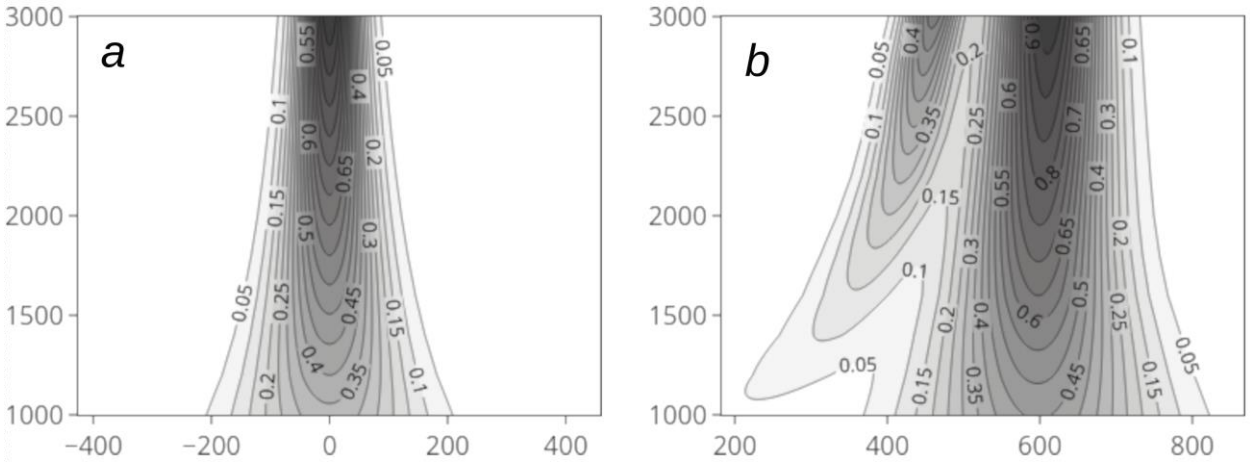

Figure 1. Horizontal BP of the RATAN-600 AS "South sector+Periscope" in the 1–3 GHz range when the receiver is in focus (*a*) and when out of focus by 430 mm (*b*). Along the horizontal axis are arcseconds; along the vertical one, the frequency in MHz

If the magnetic field was to be directed parallel to the line of sight, the σ component would be observed in the absorption in one of the circular polarizations. If the magnetic field was not to exceed 20 G, there would be a σ^+-component signal in the second circular polarization. In addition, in both circular polarizations there would be signals of equal amplitude with a π component not shifted in frequency.

If the magnetic field was to be perpendicular to the line of sight, in both circular polarizations there would be equal-amplitude σ^--component signals; if the magnetic field was not to exceed 20 G, there would be equal-amplitude σ^+-component signals.

In intermediate cases, signals with frequencies f_0, $f_0 \pm \Delta f$ will be observed in both polarizations, and their amplitudes will depend on the angle between the magnetic field direction and the line of sight.

For the above observations, the shift in the 1.65–1.67 GHz lines was 70–100 MHz, which corresponds to a field ~50–70 G, 80 MHz (~60 G), and 30 MHz (~20 G).

On January 29, 2024, coronal rain was seen on the west limb of the Sun over AR NOAA 13559. Figure 2, *b* exhibits spectrograms of full-disk radio emission in the 1.0–1.7 GHz range in two polarizations, compared with an SDO/AIA304 Å image (Figure 2, *a*), tilted according to the positional angle of the RATAN-600 BP; at 1600 MHz, the horizontal BP is 157″. Figure 2, *c* presents spectra of the selected coronal rain region (from +940″ to +1100″ from the solar disk center in the direction perpendicular to the BP vertical axis). In the 1.567–1.598 GHz region there is a shifting absorption line whose minimum presumably corresponds to the central hydroxyl line (1.665–1.667 GHz). The shift in the line position by 60–100 MHz is caused by a strong magnetic field, which drives the formation of coronal rain.

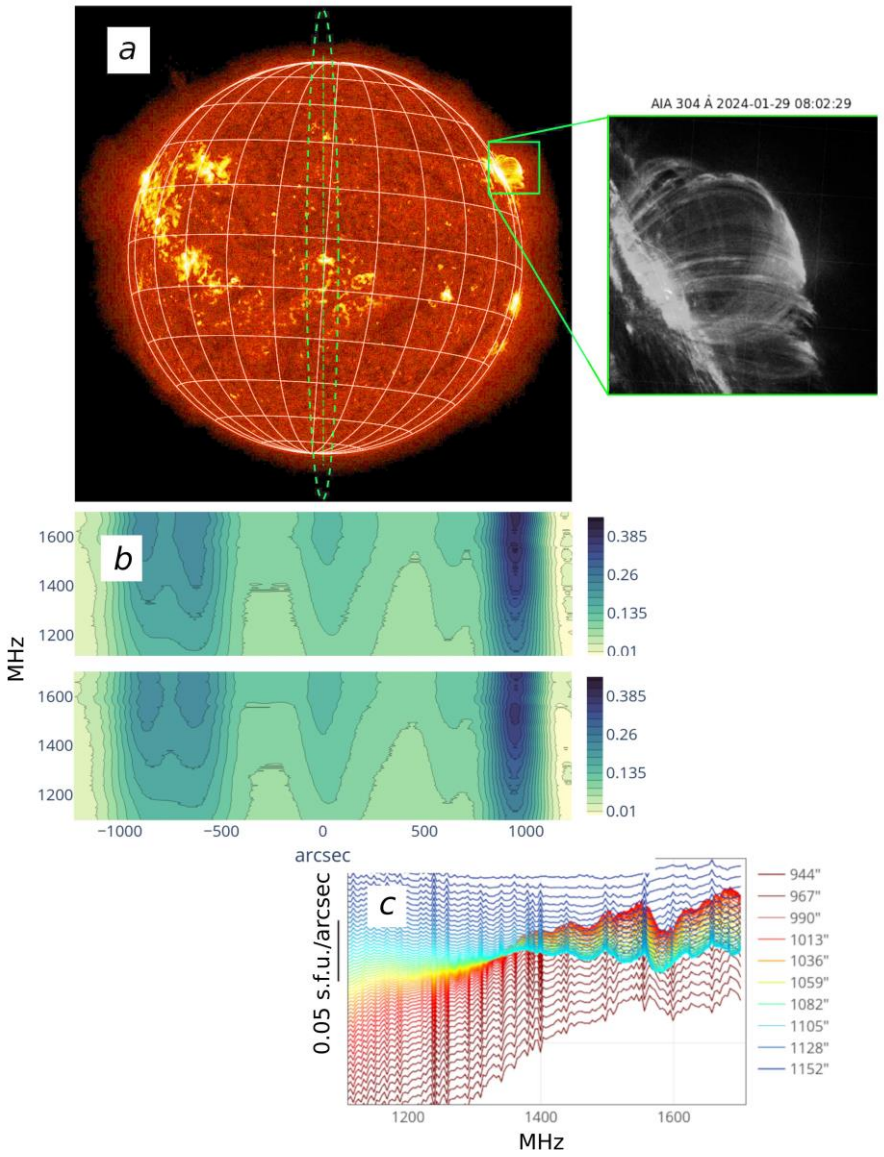

Figure 2. Observations on January 29, 2024: *a* — SDO/AIA 304 Å image; the dashed line indicates the BP position at 1600 MHz when it passes along the azimuth axis in transit mode; *b* — spectrogram of the Sun in transit in two polarizations after deconvolution with BP; *c* — radio emission spectra after deconvolution with BP from +940″ to +1100″ from the solar disk center, which corresponds to coronal rain (in the inset)

Absorption lines at 1.59–1.61 GHz and 1.65–1.68 GHz were observed in the emission from AR NOAA 13030 with a filament on June 18, 2022 on the solar disk and on June 24, 2022 when the same AR appeared on the west limb with a prominence. The observational results are shown in Figures 3 and 4 respectively.

In February 2024, there were 1.59–1.645 GHz absorption lines in the emission from AR NOAA 13586 on the limb with a filament transforming into a prominence (Figure 5).

On March 21, 2024, the absorption line in the radio emission from AR NOAA 13614 with a filament was observed both in transit mode and in tracking mode with a frequency resolution of 4 MHz. The observational results are presented in Figure 6. Figure 6, *d* shows the radio emission spectrum of AR NOAA 13614 when tracked for 7 min (09:01:34–09:08:34 UTC), excluding quiet-Sun radiation and AR thermal bremsstrahlung. According to [Maeda et al., 2015], the magnetic field in the observed region can be estimated at ~50–60 G.

To estimate the absorption, we use data from the HITRAN spectroscopic database [Gordon et al., 2022], which contains data on the spectral line intensity $S_{ij}(T_{\text{ref}})$ for the temperature $T_{\text{ref}} = 296\,\text{K}$ and Tables of partition functions.

The tabular partition function values are $Q(296\ \text{K}) = 80.34827$, $Q(5000\ \text{K}) = 2524.97805$.

For T, $S_{ij}(T)$ can be obtained from the formula

$$S_{ij}(T) = S_{ij}(T_{\text{ref}}) \frac{Q(T_{\text{ref}})}{Q(T)} \frac{e^{-c_2 E_l / T}}{e^{-c_2 E_l / T_{\text{ref}}}} \frac{1 - e^{-c_2 \nu_{ij} / T}}{1 - e^{-c_2 \nu_{ij} / T_{\text{ref}}}},$$

where $Q(T)$ is the partition function for a given substance at T; ν_{ij} is the wave number for the line considered; $c_2 = hc/k$; h is the Planck constant; c is the speed of light; k is the Boltzmann constant.

Wave absorption coefficient ν

$$\alpha(\nu, T) = S_{ij}(T)\, f(\nu, T),$$

where $f(\nu, T)$ is the spectral line shape

$$f(\nu, T) = \sqrt{\frac{\ln 2}{\pi w^2(T)}}\, e^{-\frac{(\nu - \nu_{ij})^2 \ln 2}{w^2(T)}},$$

$w(T)$ *is* half width at half maximum of the line

$$w(T) = \frac{\nu_{ij}}{c} \sqrt{\frac{2kT \ln 2 N_{\text{A}}}{M}},$$

N_{A} is the Avogadro number; M is the molecular weight.

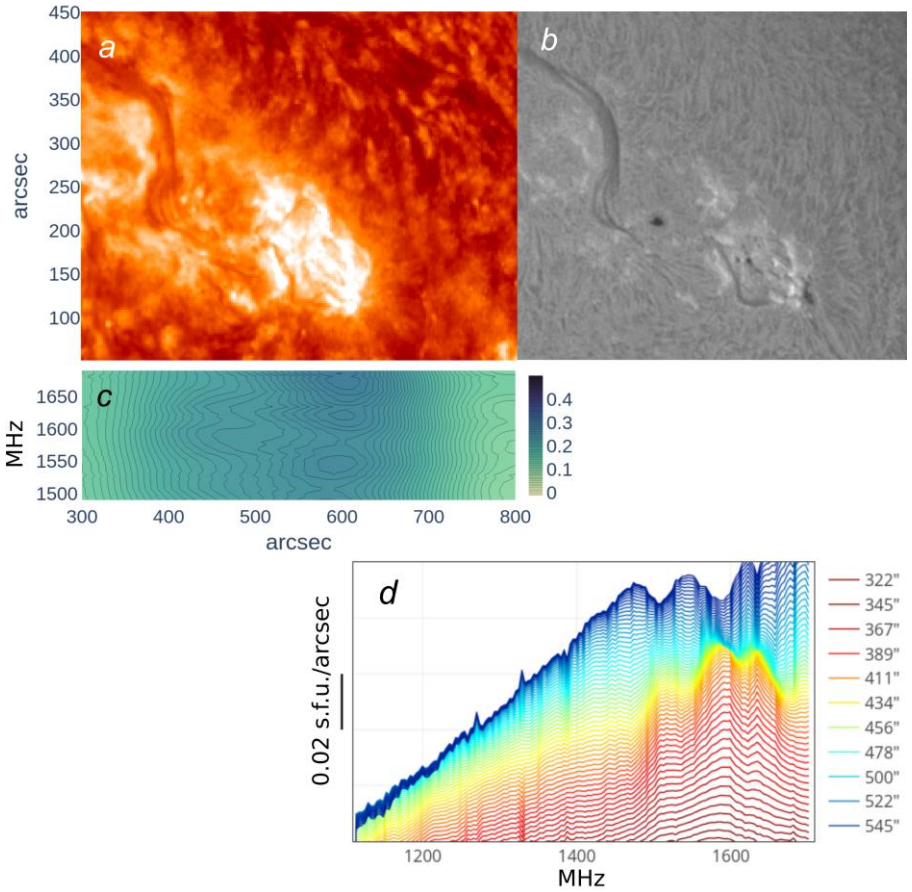

Figure 3. Observations of AR NOAA 13030 with filament on the solar disk on June 18, 2022: *a*, *b* — AR images of SDO/AIA 304 Å and GONG Ha/6562.8 Å (El Teide) respectively; *c* — spectrogram of AR radio emission in transit in left-hand polarization after deconvolution with BP; *d* — AR radio emission spectra after deconvolution with BP (from +322″ to +545″ from the solar disk center)

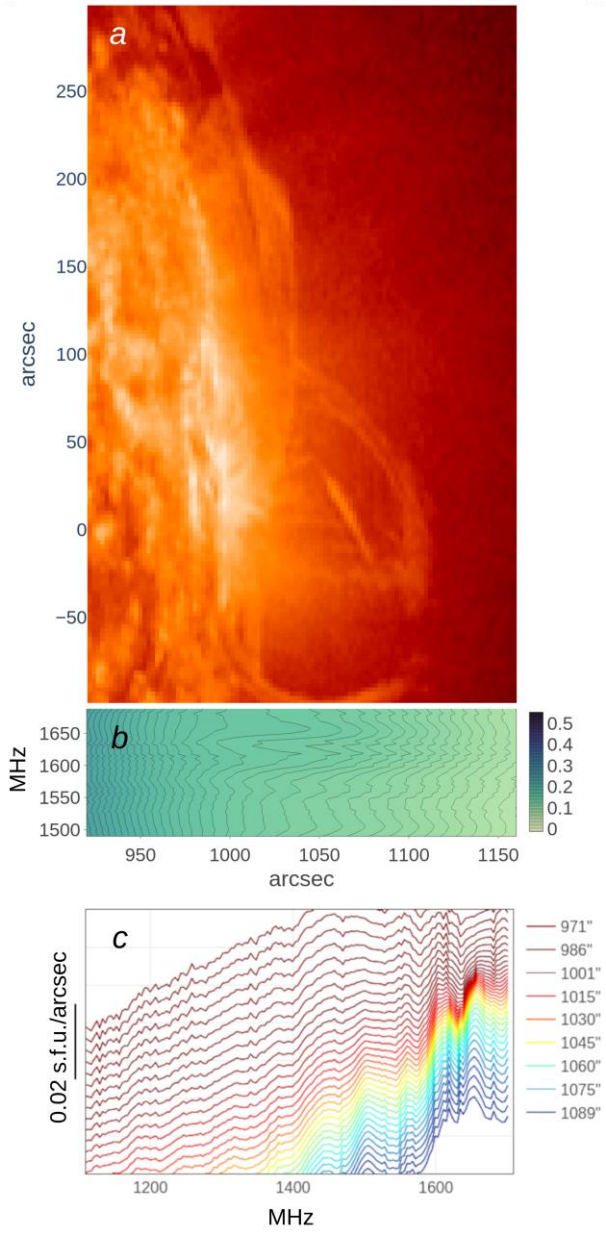

Figure 4. Observations of AR NOAA 13030 on the limb with a prominence on June 24, 2022: *a* — SDO/AIA 304 Å AR image; *b* — spectrogram of AR radio emission in transit in the right-hand polarization after deconvolution with BP; *c* — AR radio emission spectra after deconvolution with BP (from +970″ to +1090″ from the solar disk center)

Absorption in the medium is determined by the Beer—Lambert law:

$$\frac{I}{I_0} e^{-\alpha(\nu,T)u},$$

where I is the intensity of the emission transmitted through the layer of medium; I_0 is the emission intensity at the entrance to the layer of medium; u is the column density:

$$u = \int_0^l n(l)\,dl,$$

where $n(l)$ is the volumetric density. In particular, if $n(l)=const$, $u=nL$, where L is the layer thickness.

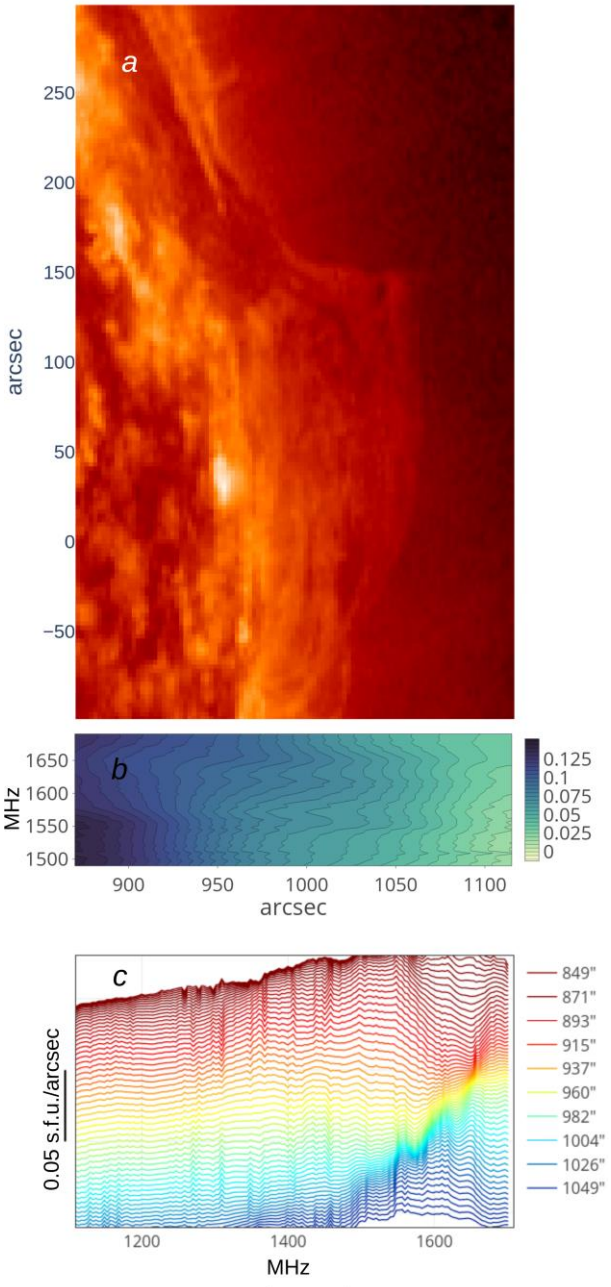

Figure 5. NOAA 13586 observations on the limb with a filament transforming into a prominence on February 25, 2024: *a* — SDO/AIA 304 Å AR image; *b* — spectrogram of AR radio emission after deconvolution with BP; *c* — AR radio emission spectra after deconvolution with BP (from +849″ to +1049″ from the solar disk center)

The oxygen content in the photosphere logϵ(O) is ~8.8 dex [Bergemann et al., 2021]. We estimated the filament height (when it appeared on the limb) at ~15 000 km. Assuming that all oxygen in the filament thickness is bonded to hydrogen, for a temperature of ~5000 K [Park et al., 2013; Sanetaka Okada et al., 2020] we get an upper absorption estimate at ~0.15 % for a line width of ~20 MHz.

This corresponds in order of magnitude to the values obtained from observations on March 21, 2024 in tracking mode: the spectral flux density in AR 13614 was 15.4–17.4 s.f.u., whereas absorption can be estimated at ~0.25 s.f.u. (see Figure 6, *d*) with a line width of ~40 MHz.

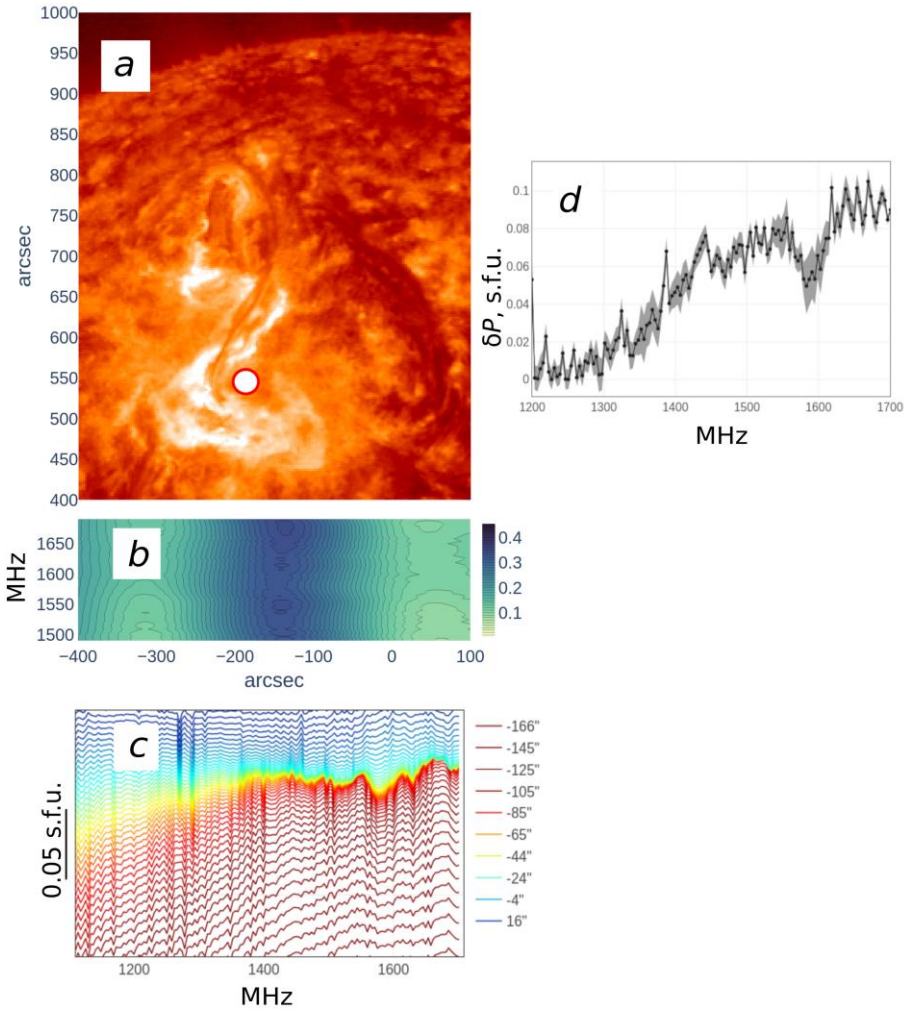

Figure 6. Observations of AR NOAA 13614 on March 21, 2024: *a* — an SDO/AIA 304 Å image (the circle indicates the tracked position of the RATAN-600 BP cente); *b* — spectrogram of AR radio emission in transit mode; *c* — AR radio emission spectra (from –166″ to +16″ from the solar disk center); *d* — averaged filament spectrum in AR NOAA 13614 with a 4 MHz resolution, obtained during tracking from 09:01:34 to 09:08:34 UTC; the achieved sensitivity can be assessed at 0.01 s.f.u.

CONCLUSION

Increasing the receiver sensitivity by using a new generation equipment with a high frequency resolution and an observation mode with signal accumulation due to long-term tracking of the source in combination with statistical data analysis methods opens up the possibility for studying minor signal variations against the background of intense solar radio emission. For the first time in the world practice, we managed to detect individual spectral lines in the radio frequency band in the solar corona. The recent observational data obtained in January–March 2024 confirms our previous results [Ovchinnikova et al., 2023]. The above estimates of absorption and line width suggest that the absorption we observed at 1.5–1.7 GHz can be explained by the presence of hydroxyl in dense cold structures in the corona.

Observations by SAO RAS telescopes are supported by the Ministry of Science and Higher Education of the Russian Federation. The renovation of telescope equipment is currently provided within the national project "Science and Universities".

REFERENCES

Bergemann M., Hoppe R., Semenova E., Carlsson M., Yakovleva S.A., Voronov Ya.V., et al. Solar oxygen abundance. *Monthly Notices of the Royal Astronomical Society*. 2021, vol. 508, iss. 2, pp. 2236–2253. DOI: 10.1093/mnras/stab2160.

Derouich M. Inversion of Zeeman polarization for solar magnetic field diagnostics. *New Astronomy*. 2017, vol. 53, pp. 26–34. DOI: 10.1016/j.newast.2016.11.007.

Dravskih A.F., Dravskih Yu.A. *Astronomicheskii Zhurnal*. 2022, vol. 99, no. 6, pp. 496–50547. DOI: 10.31857/S0004629922060032. (In Russian).

Gordon L.S., Rothman L.S., Hargreaves R.J., Hashemi R., Karlovets E.V., Skinner F.M., et al.. The HITRAN2020 molecular spectroscopic database. *Journal of Quantitative Spectroscopy and Radiative Transfer*. 2022, vol. 277, pp. 31–42. DOI: 10.1016/j.jqsrt.2021.107949.

Heyer M.H., Schloerb F.P. Application of principal component analysis to large-scale spectral line imaging studies of the interstellar medium. *Astrophys. J.* 1997, vol. 475, no. 1, pp. 173–187. DOI: 10.1086/303514.

Jaeggli S.A., Lin H., Uitenbroek H. On molecular hydrogen formation and the magnetohydrostatic equilibrium of sunspots. *Astrophys. J.* 2012, vol. 745, no. 2, article id. 133. 16 p. DOI: 10.1088/0004-637X/745/2/133.

Khersonskii V.K., Varshalovich D.A. The possibility of observing recombination lines in solar radiation. *Astronomy Rep*. 1980, vol. 24, no. 5-6, pp. 359–360.

Maeda K., Wall M.L., Carr L.D. Hyperfine structure of the hydroxyl free radical (OH) in electric and magnetic fields. *New J. Phys*. 2015, vol. 17, 045014. DOI: 10.1088/1367-2630/17/4/045014.

Ovchinnikova N.E., Lebedev M.K., Bogod V.M., Ripak A.M., Storozhenko A.A. Results of a new approach to the analysis of multi-wavelength observations data obtained with RATAN-600. *Proc. The Multifaceted Universe: Theory and Observations. PoS(MUTO2022)*. 2022, p. 425.

Ovchinnikova N.E., Bogod V.M., Lebedev M.K. Detection of hydroxyl (OH) absorption line in the radio emission of the solar corona, in proceedings of XXVII National Annual Conference “Solar and Solar-Terrestrial Physics — 2023”. Saint Petersburg, 2023, p. 245.

Park H., Chae J., Song D., Maurya R.A., Yang H., Park Y.D., et al. Temperature of solar prominences obtained with the fast imaging solar spectrograph on the 1.6 m New Solar Telescope at the Big Bear Solar Observatory. *Initial Results from the Fast Imaging Solar Spectrograph (FISS)*. Cham. 2013, pp. 105–116. DOI: 10.1007/978-3-319-12123-9_7.

Ripak A.M., Bogod V.M., Grenkov S.A. Lebedev M.K. RFI-Resistant Decimeter Band Radiometer for the RATAN-600 Radio Telescope. *Astrophys. Bull*. 2023, vol. 78, no. 4, pp. 622–634. DOI: 10.1134/S1990 341323600291.

Sanetaka Okada, Kiyoshi Ichimoto, Aki Machida, Satomi Tokuda,Yuwei Huang, Satoru Ueno. Temperature analysis of solar prominences by multi-wavelength observations. *Publ. Astron. Soc. Japan*. 2020, vol. 72, iss. 5, 71. DOI: 10.1093/pasj/psaa014.

Smilde A.K., Bro R., Geladi P. Multi-way analysis: applications in the chemical sciences. *John Wiley & Sons*. 2005.

Wild J.P. The radio-frequency line spectrum of atomic hydrogen and its applications in astronomy. *Astrophys. J.* 1952, vol. 115, p. 206. DOI: 10.1086/145533.

Zirin H., Baumert B.M., Hurford G.J. The microwave brightness temperature spectrum of the quiet sun. *Astrophys. J.* 1991, vol. 370, pp. 779–783. DOI: 10.1086/169861.

This paper is based on material presented at the 19th Annual Conference on Plasma Physics in Solar System, February 5–9, 2024, IKI RAS, Moscow.

Original Russian version: Ovchinnikova N.E., Bogod V.M., Lebedev M.K., published in Solnechno-zemnaya fizika. 2024. Vol. 10. No. 3. P. 21–26. DOI: 10.12737/szf-103202403. © 2024 INFRA-M Academic Publishing House (Nauchno-Izdatelskii Tsentr INFRA-M)

How to cite this article

Ovchinnikova N.E., Bogod V.M., Lebedev M.K. Observation at radio frequencies of the hydroxyl (OH) absorption line in filaments and prominences above active regions of the Sun. *Solar-Terrestrial Physics*. 2024. Vol. 10, Iss. 3. P. 18–24. DOI: 10.12737/stp-103202403.